HOSTED BY

ELSEVIER

CrossMark

Available online at www.sciencedirect.com

ScienceDirect

Progress in Natural Science: Materials International 25 (2015) 6–11

Progress in Natural Science Materials International

www.elsevier.com/locate/pnsmi
www.sciencedirect.com

Original Research

Gd–La codoped TiO_2 nanoparticles as solar photocatalysts

Meng Wang[a,1], Xiaoyu Xu[a,1], Lin Lin[b,*], Dannong He[a,b,**]

[a]School of Materials Science and Engineering, Shanghai Jiao Tong University, 200240 Shanghai, China
[b]National Engineering Research Center for Nanotechnology, 200241 Shanghai, China

Received 20 June 2014; accepted 1 December 2014
Available online 20 February 2015

Abstract

Gd–La codoped TiO_2 nanoparticles with diameter of 10 nm were successfully synthesized via a sol–gel method. The photocatalytic activity of the Gd–La codoped TiO_2 nanoparticles evaluated by photodegrading methyl orange was significantly enhanced compared to that of undoped or Gd or La mono-doped TiO_2. Ti^{4+} may substitute for La^{3+} and Gd^{3+} in the lattices of rare earth oxides to create abundant oxygen vacancies and surface defects for electron trapping and dye adsorption, accelerating the separation of photogenerated electron–hole pairs and methyl orange photodegradation. It is believed that the formation of an excitation energy level below the conduction band of TiO_2 from the binding of electrons and oxygen vacancies decreases the excitation energy of Gd–La codoped TiO_2, resulting in versatile solar photocatalysts. The results suggest that Gd–La codoped TiO_2 nanoparticles are promising for future solar photocatalysts.

Keywords: Photocatalyst; Titaninm dioxide; Semiconductor; Photodegradation; Nanotechnology

1. Introduction

It is widely recognized that the photocatalytic technology from semiconductor materials provides a feasible route to environmental pollution control and energy harvesting [1–6]. Among plentiful semiconductor materials, titania (TiO_2) nanostructures are believed to be the most promising catalysts in photocatalysis, hydrogen generation, and anode electrodes of photovoltaic cells because of their versatile properties in nature: clean, non-polluting, inexhaustible, biocompatible, and low-price [7]. However, the main drawbacks of TiO_2 nanostructures that limit their commercial applications are the fast recombination of photogenerated electron–hole pairs and the UV-response only due to their wide bandgap energy [8]. By addressing these issues, many attempts have been made to enhance the photocatalytic activity of TiO_2 nanostructures by improving the electron–hole separation and extending the optical absorption to the visible-light region by surface modification, structure optimization, doping of noble metal or nonmetal elements.

Different from the traditional approaches of extending absorption wavelength range of TiO_2 photocatalysts, we have recently investigated Gd–La codoped TiO_2 nanostructures as efficient solar phosphors. The codoped La and Gd elements serve as intermediums, which are substituted by Ti to create abundant oxygen vacancies and surface defects for efficient separation of photogenerated electron–hole pairs and dye adsorption. More importantly, the oxygen vacancies can easily bind with electrons to form an excitation energy level below the conduction band of TiO_2, which results in an efficient solar-light absorption. The early works on using rare earth doped TiO_2 as photocatalysts were mainly focused on the doping of TiO_2 by mono-rare earth element, such as Gd [9], La [10], Yb [8], Er [11], or Ce [12]. However, the doping of TiO_2 by mono-rare earth either enhances the separation of photogenerated electron–hole pairs or extends absorption wavelength span of TiO_2. By combining TiO_2 base with bi-rare earth elements, the limits of mono-doping issues can be efficiently compensated.

*Corresponding author. Tel.: +86 21 34291286; fax: +86 21 34291125.
**Corresponding author at: National Engineering Research Center for Nanotechnology, 200241 Shanghai, China. Tel.: +86 21 34291286; fax: +86 21 34291125.
E-mail addresses: linlin21023@163.com (L. Lin), hdnbill@sh163.net (D. He).
[1]These authors contribute equally to this work.
Peer review under responsibility of Chinese Materials Research Society.

http://dx.doi.org/10.1016/j.pnsc.2015.01.002

In search for more promising photocatalysts, here we report the study of Gd–La codoped TiO_2 nanostructures as efficient solar photocatalyst candidates for dye photodegradation. To the best of our knowledge, there are still few reports on the employment of Gd–La codoped TiO_2 nanoparticles as solar photocatalysts.

2. Experimental

2.1. Synthesis of Gd–La codoped TiO_2 nanoparticles

Gd–La codoped TiO_2 nanoparticles were synthesizedvia a sol–gel method. In details, 10 ml of tetra-*n*-butyl titanium was dissolved in a mixture of 80 ml of anhydrous ethanol, 1 ml of concentrated nitric acid and 2 ml of deionized water and stirred for 1 h at room temperature. Under vigorous agitation, lanthanum nitrate and gadolinium nitrate were added to the above mixture according to stoichiometric molar proportion. After 1 h, a stable, transparent solution was obtained. The resultant gel was further prepared by keeping the sol at room temperature for 4 h. After being dried at 80 °C for 12 h, the powders were milled and calcined in a muffle furnace of 450 °C for 3 h at a heating rate of 2 °C min^{-1}.Finally, the Gd–La codoped TiO_2 photocatalysts were obtained and kept in a sealed vessel for future characterizations. As references, the undoped, Gd or La mono-doped TiO_2 nanoparticles were also prepared under the same conditions.

2.2. Photocatalytic performances of the Gd–La codoped TiO_2 photocatalysts

The photodegradation reactions were carried out under atmospheric condition using 500 W xenon lamps as UV-light source. A 420 nm cutoff filter with more than 90% transmission was employed in order to obtain visible light, and simulated AM 1.5 G solar illumination at 100 mW cm^{-2} from a xenon arc lamp (CHFXM500,Trusttech Co., Ltd., China) as sunlight source at ambient conditions. The irradiation distance between lamp and the sample was 10 cm. 0.1 g of Gd–La codoped TiO_2 photocatalysts were added into a cylindrical glass vessel containing 100 ml of MO aqueous solution with a concentration of 20 mg L^{-1}. Before exposing the sample to the light source, the MO aqueous solution was agitated thoroughly with the catalyst slide in the dark for 30 min to reach the adsorption equilibrium of the dye on the catalyst. At an interval of 10 min and UV-irradiation, the photodegradation reaction was ceased and the solution was centrifuged, whereas the interval was 20 min at visible-light irradiation. The residual dye concentration in the supernatant was measured by a UV–vis spectrometer (Lambda850) at maximum absorption wavelength of 460 nm for MO. As a comparison, the photocatalytic activities of undoped, La or Gd mono-doped TiO_2 were also measured under the same conditions.

2.3. Characterizations

The morphology was observed on a TEM (JEM2010, JEOL).The crystal structure of the as-prepared catalysts were characterized by an XRD [X'pert MPD Pro, Philips, Netherlands with Cu*K*α radiation ($\lambda = 0.15418$ nm) in the 2θ range from 5° to 70° operating at 40 kV accelerating voltage and 40 mA current]. The optical absorption spectra were recorded on a UV–vis spectrophotometer (Agilent 8453) at room temperature. Fourier transformed Raman spectroscopic measurements in the ultraviolet light were performed on a Renishawin via Reflex Raman Spectrometer. High-resolution gratings were used to give a spectral resolution of 2 cm^{-1}. The spectra were recorded at room temperature from 3200 to 100 cm^{-1} using 16 scans with an exposure time of 1 s per scan. XPS experiments were carried out on an RBD upgraded PHI-5000C ESCA system (Perkin-Elmer) with Mg Kα radiation ($h\nu = 1253.6$ eV). In general, the X-ray anode was run at 250 W and the high voltage was kept at 14.0 kV with a detection angle at 54°. The pass energy was fixed at 23.5, 46.95 or 93.90 eV to ensure sufficient resolution and sensitivity. The base pressure of the analyzer chamber was about 5×10^{-8} Pa. The sample was directly pressed to a self-supported disk (10×10 mm^2), mounted on a sample holder, and then transferred into the analyzer chamber. Binding energies were calibrated by using the containment carbon (C1s = 284.6 eV).

3. Results and discussion

3.1. Morphology characterizations

Fig. 1a and c shows representative TEM images of undoped and Gd–La codoped TiO_2 nanoparticles, respectively. These particles exhibit average sizes from a few nanometers to several tens nanometers. Fig. 1b shows HRTEM image of undoped TiO_2 nanoparticles. There is no lattice distortion in current nanoparticle and all atoms are well-aligned in the lattice. The lattice spacing of (101) atomic plane is 0.35 nm. The corresponding FFT pattern from the particle shown in Fig. 1b is demonstrated as inset in Fig. 1b. Gd–La codoped TiO_2 nanoparticles show different HRTEM view in Fig. 1d compared to that of undoped TiO_2 nanoparticles. The crystal ionic radius of Ti^{4+}, La^{3+}, and Gd^{3+} are 0.068, 0.115, and 0.0938 nm respectively. Due to the fact that the radius of Ti^{4+} is much less than that of La^{3+} and Gd^{3+}, Ti^{4+}may enter the La^{3+} and Gd^{3+} lattices during synthesis, which induces a great deal of lattice distortions and plenty of defects at and under surface of Gd–La codoped TiO_2 nanoparticles. The corresponding FFT pattern formed in Fig. 1d shows that the Gd–La codoped TiO_2 is a polycrystalline structure.

3.2. Structural analysis

XRD was usually employed for identification of the crystal phase as well as crystallite size of TiO_2. The diffraction peaks at $2\theta = 25.3$, 37.0, 37.7, 38.6, 48.0, 53.9, 55.1, 62.7, and 68.8 in the spectrum of undoped TiO_2 are identified and attributed to the diffraction faces of (101), (103), (004), (112), (200), (105), (211), (204), and (116), respectively. The results show that the crystal phase of undoped TiO_2 is anatase (Fig. 2).

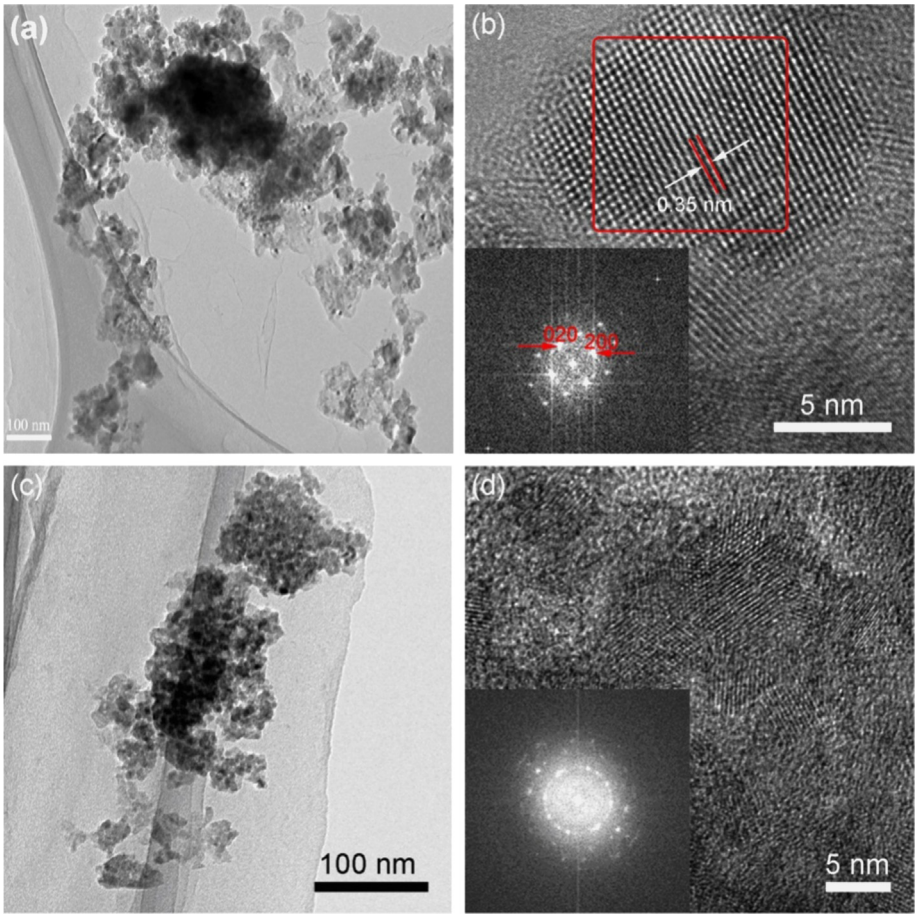

Fig. 1. (a,b) TEM and HRTEM images of undoped TiO_2 nanoparticles, inset is corresponding to FFT in (b); (c,d) TEM and HRTEM images of Gd–La codoped TiO_2 nanoparticles, inset is corresponding to FFT in (d).

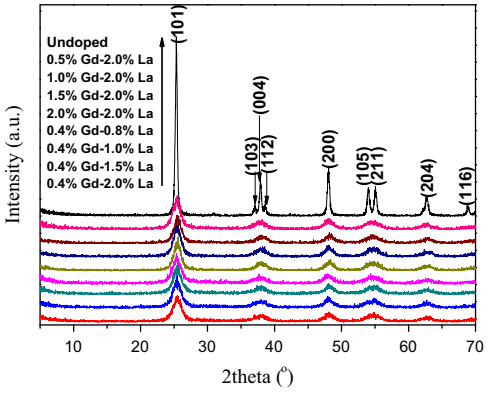

Fig. 2. XRD patterns of undoped and Gd–La codoped TiO_2 nanoparticles.

No diffraction peaks of rutile phase are detected in the XRD pattern. The crystallite size can be determined from the broadening of corresponding XRD peaks by Scherrer formula [13]

$$L = \frac{K\lambda}{\beta \cos \theta} \tag{1}$$

where L is the crystallite size, λ is the wavelength of the X-ray radiation (Cu$K\alpha$ = 0.15418 nm), K is usually taken as 0.89, and β is the line width at half-maximum height (FWHM). In addition, the crystal lattice distortion ($\Delta d/d$) can also be evaluated from the following equation [14]:

$$\frac{\Delta d}{d} = \frac{\beta}{4tg\theta} \tag{2}$$

At the first glance, all the diffraction peaks belonging to the diffraction faces of anatase TiO_2 can be detected in the Gd–La codoped TiO_2photocatalysts. However, the relative intensity of diffraction peak belonging to (101) face of anatase TiO_2 phase dramatically decreases after being codoped by Gd and La ions, indicating an inhibition effect of phase transformation from amorphous to anatase TiO_2. Moreover, the crystallite size of the Gd–La codoped TiO_2 has an order of decreasing with increase of La dosage at a Gd content of 0.4% (Table 1), suggesting that the doping of La in TiO_2 can hinder the growth of crystallite size due to the segregation of dopant cations at the grain boundary [15]. It has been well known that the ionic radii of La^{3+} (0.115 nm) and Gd^{3+} (0.0938 nm) are much bigger than that of Ti^{4+} (0.068 nm), suggesting that La^{3+} or Gd^{3+} ions cannot enter into TiO_2 crystal lattice to substitute for Ti^{4+}. However, there is a slight difference in the lattice parameters "a" and "c" between undoped and Gd–La codoped TiO_2 photocatalysts and the values of all the Gd–La codoped

Table 1
Structure parameters obtained from XRD patterns of undoped and Gd–La codoped TiO_2 photocatalysts.

Samples	FWHM (deg)	2θ (deg)	Crystallite size (nm)	Δd/d	a (nm)	c (nm)
Undoped TiO_2	0.32	25.33	25.19	0.0062	0.4983	0.4985
0.5%Gd–2.0%La/TiO_2	1.58	25.27	5.10	0.031	0.4972	0.4973
1.0%Gd–2.0%La/TiO_2	1.60	25.43	5.04	0.031	0.4953	0.4954
1.5%Gd–2.0%La/TiO_2	1.51	25.48	5.34	0.029	0.4943	0.4944
2.0%Gd–2.0%La/TiO_2	1.62	25.51	4.98	0.031	0.4937	0.4939
0.4%Gd–0.8%La/TiO_2	1.38	25.60	5.84	0.027	0.4920	0.4922
0.4%Gd–1.0%La/TiO_2	1.38	25.53	5.83	0.025	0.4933	0.4935
0.4%Gd–1.5%La/TiO_2	1.44	25.48	5.60	0.028	0.4943	0.4944
0.4%Gd–2.0%La/TiO_2	1.46	25.44	5.52	0.028	0.4951	0.4952

TiO_2 are less than that of undoped TiO_2. At the interfaces, Ti^{4+} may substitute for La^{3+} and Gd^{3+} in the lattices of rare earth oxides to decrease the lattice parameters [16], which is consistent with the morphology analysis.

Crystallographic structure of the Gd–La codoped TiO_2 nanoparticles was judged by Raman spectroscopy and shown in Fig. 3. As a comparison, the Raman spectra of the undoped, 1.5% La doped, and 0.4% Gd doped TiO_2 were also conducted. The Raman bands at 148, 395, 514, and 639 cm^{-1} in the codoped TiO_2 are attributed to $E_g(1)$, $B_{1g}(1)$, $A_{1g}/B_{1g}(2)$, and $E_g(3)$ modes of anatase phase of TiO_2 (Table 2), respectively. The conclusion is consistent with that of XRD analysis. No Raman peaks corresponding to Gd_2O_3 and La_2O_3 can be detected in the doped TiO_2, indicating that Ti^{4+} may be present in the substitutional positions in the crystal lattices of Gd_2O_3 and La_2O_3. However, the mode positions have shifted in comparison with undoped TiO_2. It is attributed to the decrease in crystallite size (Table 1) and lack of adjacent atoms for the surface atoms. Therefore, the surface atoms are in a relaxation state and the red-shift results from a surface relaxation effect [17].

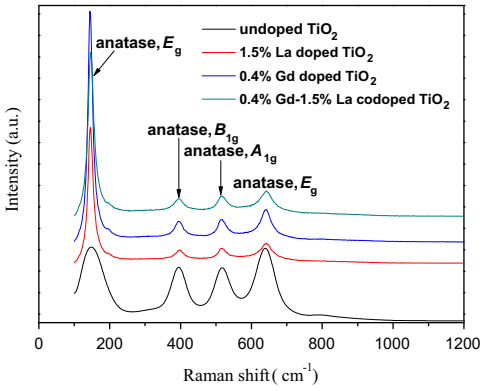

Fig. 3. Raman spectra of the undoped, 1.5% La doped, 0.4% Gd doped, and 0.4% Gd–1.5% La codopedTiO_2 nanoparticles.

Table 2
Assignments of Raman bands (cm^{-1}) of undoped, 1.5% La doped, 0.4% Gd doped, and 0.4% Gd–1.5% La codoped TiO_2 nanoparticles.

Undoped	1.5% La doped	0.4% Gd doped	0.4% Gd–1.5% La codoped	Mode
148	146	145	146	$E_g(1)$
395	397	397	397	$B_{1g}(1)$
514	516	516	516	A_{1g}, $B_{1g}(2)$
639	643	643	641	$E_g(3)$

3.3. Photocatalytic activity

Fig. 4a–c shows the decrease of MO concentration at various irradiation times. Under UV-irradiation, MO molecules were photodegraded slowly due to the photosensitization of undoped TiO_2. The photocatalytic activities of the Gd and La doped TiO_2 at various dosages were also depicted as references to evaluate the activity of the doped TiO_2, showing significant enhancement in photocatalytic activity. It was found that 0.4% Gd–1.5% La codoped TiO_2 presented the highest photocatalytic activity, which would be an optimum dose for the Gd–La codopedTiO_2. Similarly, when under visible and solar light irradiations, the presence of undoped TiO_2 had no notable effect on the photodegradation of MO, whereas the 0.4% Gd and 1.5% La doped TiO_2 exhibited much higher photocatalytic activity than that of undoped TiO_2. However, the photocatalytic activity was further enhanced by codoping 0.4% Gd and 1.5% La into TiO_2. But the increment of the doping dosage did not necessarily suggest a better photocatalytic activity, for the redundant doping ions would become the recombination center of the photogenerated electrons and holes, which was unfavorable for the photodegradation.

The kinetics of the photodegradation of MO in the presence of the undoped, 0.4% Gd doped, 1.5% La doped, and 0.4% Gd–1.5% La codoped TiO_2 were also studied. The $\ln(C/C_0)$ of these samples present good linear reaction with the irradiation time (shown in Fig. 4(d) and (e)), which means that the photodegradation of MO obeys the rules of a first-order reaction kinectics $-\ln(C/C_0)=kt$. The reaction rate constants k of the photodegradation of MO from 0.4% Gd–1.5% La codoped TiO_2 is the highest. Therefore, we can conclude that 0.4% Gd–1.5% La codoped TiO_2 nanoparticles are believed to be the best solar photocatalysts.

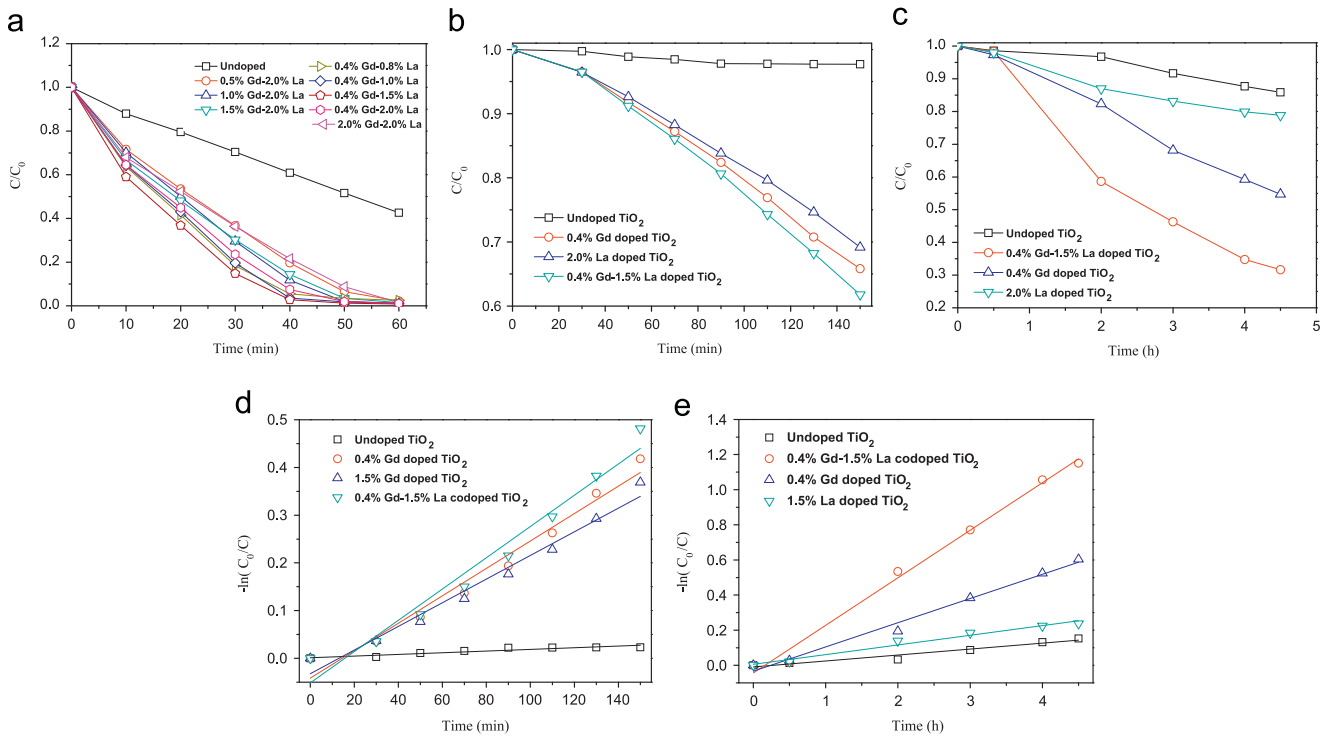

Fig. 4. Time course of the decrease in the concentration for the photodegradation of MO by undoped,Gd doped, La doped, and Gd–La codoped TiO_2 nanoparticles under (a) ultraviolet, (b) visible, and (c) solar irradiations. (d) and (e) are the relationships between $\ln(C_0/C)$ and time under visible and solar irradiations, respectively.

The surface chemical state of Gd–La codoped TiO_2 catalysts and their effect on the photodegradation performance were also studied in this work. As can be seen from Fig. 5, Ti $2p_{3/2}$ peak was detected and there was a slight shift to the lower binding energy direction when codoped, from 458.9 ev to 457.7 ev, which indicated the transformation from Ti^{4+} to Ti^{3+} in the surface of the photocatalyst [18]. Similarly, the O 1s peak located at 530.5 eV agreed with the electron binding energy for TiO_2 in the undoped TiO_2, whereas the peak position at 529.1 eV in Gd–La codoped TiO_2 meant the presence of Ti_2O_3 [16]. The generated Ti^{3+} can act as defects in the TiO_2 catalysts. These defects can inhibit the recombination of electron–hole pairs and therefore expand the lifetime of the charges [19], which mean a higher photocatalytic activity.

The photocatalytic performance can also be confirmed by the UV–vis diffuse reflection spectrum in Fig. 6. After doping, a blue-shift, attributing to the quantum size effect [14], was detected, suggesting that the doping of La, Gd, or Gd–La could give rise to new spectrum phenomena as well as inhibit the growth of anatase crystallite. The results were in good agreement with XRD analysis. Moreover, the absorption intensity was significantly enhanced by doping rare earth elements, specially the codoping of Gd–La, which indicated the photogeneration of more electron–hole pairs under the light irradiation and explained the high photocatalytic performance.

In addition, it has been reported that there is an important effect of La element on dye adsorption in La doped TiO_2 because La elements can form complexes with various Lewis bases e.g. acids, amines, aldehydes, alcohols, thiols, etc. [9,20]. Moreover, the incorporation of Gd^{3+} into TiO_2 can shorten the distance of charge transfer and therefore enhance photocatalytic activity [9]. Under the irradiation of solar light, the charges can be easily photogenerated because of the decrease of bandgap, as depicted in Fig. 7. They are also the reasons to improve the photocatalytic activity via doping.

4. Conclusions

The fabrication of efficient Gd–La codoped TiO_2 nanoparticles for photocatalysts have been demonstrated. The photocatalytic degradation of MO revealed that Gd–La codoped TiO_2 can work more efficiently as photocatalysts in comparison to undoped and Gd or La doped TiO_2 nanoparticles. Ti^{4+} substitute for La^{3+} and Gd^{3+} in the crystal lattices of La_2O_3 and Gd_2O_3 to create abundant oxygen vacancies and surface defects. The oxygen vacancies can easily bind electrons to form an exciton energy level below the conduction band of TiO_2, resulting in an efficiently photocatalytic activity under solar light irradiation. However, the surface defects provide active sites to adsorb MO molecules which shortens the transfer distance of photogenerated charges. A preliminary research on photocatalytic performances reveals a significant enhancement in the photodegradation of MO under solar irradiation by Gd–La codoping and obeys the rules of a first-order reaction kinectics. The insight into the effect of lower exciton energy on charge separation and excitation was proposed, providing a promising platform for fabricating highly efficient solar photocatalysts or anodes for photovoltaic cells.

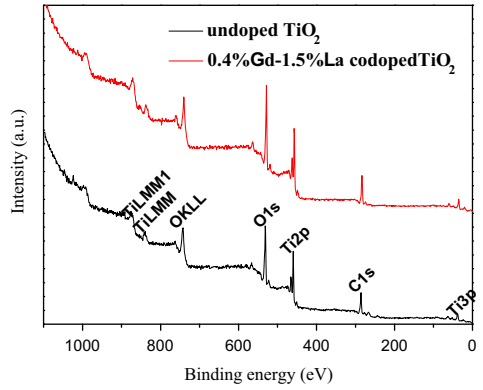

Fig. 5. XPS spectra of undoped and Gd–La codoped TiO_2 nanoparticles.

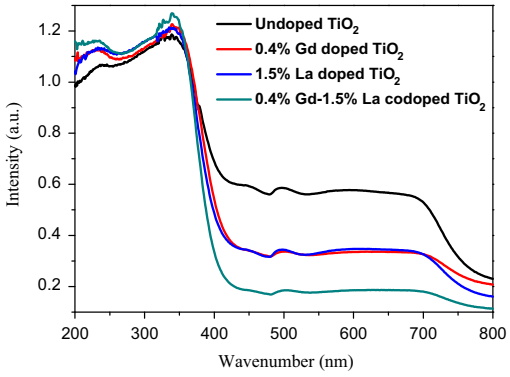

Fig. 6. UV–vis diffuse reflection spectra of undoped, 1.5% La doped, 0.4% Gd doped, and 0.4% Gd–1.5% La codoped TiO_2 nanoparticles.

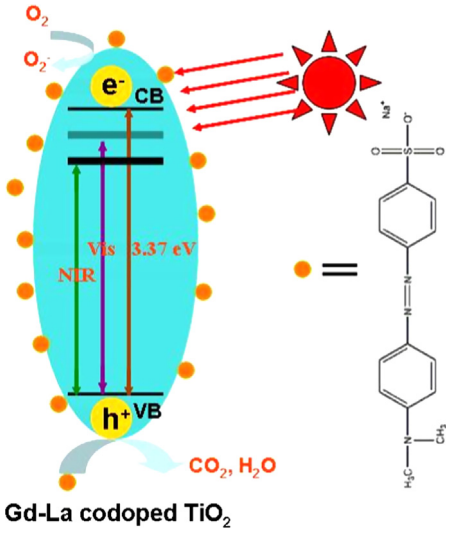

Fig. 7. Schematic of the solar light induced photodegradation in the Gd–La codoped TiO_2 photocatalysts.

Acknowledgments

The work was supported by the Shanghai Municipal Natural Science Foundation (No. 13ZR1429300), the Basic Research Program of Shanghai Science and Technology Committee (No. 13NM1401600), and the Shanghai Committee of Science and Technology (No. 12nm0504800).

References

[1] J.H. Wu, J.L. Wang, J.M. Lin, Z. Lan, Q.W. Tang, M.L. Huang, Y.F. Huang, L.Q. Fan, Q.B. Li, Z.Y. Tang, Adv. Energy Mater. 2 (2012) 78–81.
[2] L. Pan, J.J. Zou, X.W. Zhang, L. Wang, J. Am. Chem. Soc. 133 (2011) 10000–10002.
[3] Z.J. Gu, Y.C. Yang, K.Y. Li, X.Y. Tao, G. Eres, J.Y. Howe, L.T. Zhang, X.D. Li, Z.W. Pan, Carbon 49 (2011) 2475–2482.
[4] H. Zhou, X.F. Li, T.X. Fan, F.E. Osterloh, J. Ding, E.M. Sabio, D. Zhang, Q.X. Guo, Adv. Mater. 22 (2010) 951–956.
[5] X.F. Li, T.X. Fan, H. Zhou, S.K. Chow, W. Zhang, D. Zhang, Q.X. Guo, H. Ogawa, Adv. Funct. Mater. 19 (2009) 45–56.
[6] G.Q. Zhang, S. Finefrock, D.X. Liang, G.G. Yadav, H.R. Yang, H.Y. Fang, Y. Wu, Nanoscale 3 (2011) 2430–2443.
[7] J.H. Park, S. Kim, A.J. Bard, Nano Lett. 6 (2006) 24–28.
[8] Z.X. Li, F.B. Shi, T. Zhang, H.S. Wu, L.D. Sun, C.H. Yan, Chem. Commun. 47 (2011) 8109–8111.
[9] K.V. Baiju, P. Periyat, P. Shajesh, W. Wunderlich, K.A. Manjumol, V.S. Smitha, K.B. Jaimy, K.G.K. Warrier, J. Alloy Compd. 505 (2010) 194–200.
[10] S. Anandan, Y. Ikuma, V. Murugesan, Int. J. Photoenergy 2012 (2012) 780562.
[11] S. Obregón, G. Colón, Chem. Commun. 48 (2012) 7865–7867.
[12] D.C. Romero, G.T. Torres, J.C. Arevalo, R. Gomez, A.A. Elguezabal, J. Sol–Gel Sci. Technol. 56 (2010) 219–226.
[13] Q.H. Zhang, L. Gao, J.K. Guo, Appl. Catal. B: Environ. 26 (2000) 207–215.
[14] L.Q. Jing, X.J. Sun, B.F. Xin, B.Q. Wang, W.M. Cai, H.G. Fu, J. Solid State Chem. 177 (2004) 375–3382.
[15] Y.H. Zhang, H.X. Zhang, Y.X. Xu, Y.G. Wang, J. Mater. Chem. 13 (2003) 2261–2265.
[16] F.B. Li, X.Z. Li, M.F. Hou, Appl. Catal. B: Environ. 48 (2004) 185–194.
[17] C.H. Yang, Z.Q. Ma, F. Li, B. He, J.H. Yuan, Z.H. Zhang, Acta Phys.-Chim. Sin. 26 (2010) 1349–1354.
[18] B.M. Reddy, B. Chowdhury, P.G. Smirniotis, Appl. Catal. A: Gen. 210 (2001) 53–60.
[19] G. Liu, L.-C. Yin, J. Wang, P. Niu, C. Zhen, Y. Xie, H.-M. Cheng, Energy Environ. Sci. 5 (2012) 9603–9610.
[20] E. Setiawati, K. Kawano, J. Alloy Compd. 451 (2008) 293–296.